Materials Science & Engineering A 792 (2020) 139800

Contents lists available at ScienceDirect

Materials Science & Engineering A

journal homepage: http://www.elsevier.com/locate/msea

On the characterization procedure to quantify the contribution of microstructure on mechanical properties in intercritically deformed low carbon HSLA steels

U. Mayo [a,b], N. Isasti [a,b], J.M. Rodriguez-Ibabe [a,b], P. Uranga [a,b,*]

[a] CEIT-Basque Research Technology Alliance (BRTA), Manuel Lardizabal 15, 20018, Donostia / San Sebastián, Spain
[b] Universidad de Navarra, Tecnun, Manuel Lardizabal 13, 20018, Donostia / San Sebastián, Spain

ARTICLE INFO

Keywords:
Intercritical rolling
Microalloyed steels
Microstructure
EBSD
Mechanical properties

ABSTRACT

The mechanical properties of intercritically rolled microstructures have been scarcely reported in literature. Although the strengthening effect of intercritical rolling is generally recognized, there is no a clear opinion on its effect on toughness. Therefore, a greater knowledge of how different process parameters affect the mechanical properties during intercritical deformation is required. With the aim of evaluating the relationship between microstructure and mechanical properties on intercritically deformed low carbon steels, plane strain compression tests were carried out. Plane strain compression tests allow for both the characterization of the microstructural features and the evaluation of mechanical properties, via tensile and Charpy tests. Firstly, the intercritically deformed microstructures were characterized using the EBSD technique, and then a discretization methodology was used to distinguish both intercritically deformed and non-deformed ferrite populations. Next, strength and toughness properties were measured by means of tensile and Charpy tests. The results indicate that the reduction of the deformation temperature leads to an increment of yield strength for both steels, but at the same time toughness properties worsen. Deformed ferrite fractions higher than 25% result in a very pronounced loss of ductility. The yield strength was predicted by estimating the contribution of different strengthening mechanisms (solid solution, grain size refinement, dislocation density) corresponding to each ferrite population by considering a nonlinear law of mixtures. Similarly, the impact of different microstructural parameters (solid solution, grain size, microstructural heterogeneity, contribution of dislocation density and secondary phases) on toughness was evaluated and a new equation able to predict ductile to brittle transition temperature for intercritically deformed microstructures was developed.

1. Introduction

Deformation within the intercritical or austenite/ferrite range is a process of considerable industrial importance as it leads to higher tensile properties more than those produced by deformation solely in the austenite region [1,2]. Even though strength levels can be increased by intercritical rolling, toughness properties may be impaired, because controlling the final properties is much more complex in intercritical rolling compared with conventional hot rolling.

The origin of the increased complexity is principally due to the deformation of a two-phase material composed of austenite and ferrite, which leads to a different distribution of strain and stress between both phases. Generally, when two or more phases coexist in a microstructure, the properties of the mixture depend on the characteristics of each constituent in a complex way. However, during intercritical rolling there is the possibility of several processes and softening mechanisms taking place together: austenite recovery, austenite recrystallization, deformation-induced austenite to ferrite transformation, ferrite recovery and ferrite recrystallization, increasing the difficulty in predicting the final properties.

Although the mechanisms and processes taking place in the austenite [3–8] and ferrite [9–14] regions are well understood, there is very little literature available on the interactions between both constituents in a two-phase mixture. There are some works focused on ferrite recovery and the recrystallization that occurs during deformation in the two-phase region [9–11]. Other authors studied the dynamic

* Corresponding author. CEIT-Basque Research Technology Alliance (BRTA), Manuel Lardizabal 15, 20018, Donostia / San Sebastián, Spain.
E-mail addresses: umayo@ceit.es (U. Mayo), nisasti@ceit.es (N. Isasti), jmribabe@ceit.es (J.M. Rodriguez-Ibabe), puranga@ceit.es (P. Uranga).

https://doi.org/10.1016/j.msea.2020.139800
Received 7 April 2020; Received in revised form 17 June 2020; Accepted 18 June 2020
Available online 24 June 2020
0921-5093/© 2020 Elsevier B.V. All rights reserved.

strain-induced transformation that takes place during biphasic deformation, which promotes refinement of the ferrite grain size [15,16]. Furthermore, the processing windows in intercritical rolling are very small, lower than 50 °C in most of the cases, which adds another difficulty to the control of the rolling process [11,17]. Therefore, there is no clear information about microstructure evolution throughout the whole process and the relation between the final microstructure and the measured mechanical properties.

Recent research carried out on intercritical rolling [18] in the frame of a European RFCS project, confirmed that intercritically deformed ferrite fraction affect strength positively while impairing toughness properties. Also, grain size distributions for both deformed and non-deformed families were pointed out to be a key factor for strengthening and toughness control. Under the testing conditions explored during the project, texture effect on mechanical properties were shown to be less relevant when compared to grain size [19]. In a recently published work [20], a methodology capable of distinguishing between different ferrite populations generated after simulating intercritical rolling conditions (intercritically deformed (DF) and non-deformed ferrite (NDF) formed during the final cooling) was developed for low carbon steels using EBSD. This procedure permits the quantification of different microstructural features like grain size, fraction of low and high angle boundaries, dislocation density etc. of each ferrite population (NDF and DF) individually, and it provides a better understanding of the effect of the rolling process parameters on the microstructural evolution. In a follow-up paper [21], the discretization procedure was extended and validated for microalloyed steels, and the interactions between Nb with intercritically deformed ferrite grains were explained in depth.

In order to complete the study concerning intercritical rolling performed in the previously mentioned papers [20,21], the current work is focused on the application of this EBSD characterization procedure to quantify the strengthening contributions of the microstructure in intercritically deformed low carbon steels. The paper discusses the different metallurgical phenomena taking place during two-phase deformation and explains their impact on tensile and toughness properties.

2. Experimental procedure

A low carbon steel (with 0.06% C) and a NbV microalloyed steel were selected for the current study. The chemical compositions of the steels are shown in Table 1.

Each steel grade was subjected to a different thermomechanical cycle using plane strain compression tests, as depicted schematically in Fig. 1a and b (Cycle A for the CMn and Cycle B for the NbV steel). Both cycles include a reheating step at 1250 °C for 15 min in order to dissolve all the microalloying elements in the NbV grade. In both cases, a compression deformation of 0.4 at 1 s^{-1} was applied at 1050 °C in order to obtain a recrystallized austenite prior to transformation. For the NbV steel, a second deformation pass was applied at 900 °C, which is below the non-recrystallization temperature, in order to accumulate deformation in the austenite prior to transformation. Afterwards, in both cycles the samples were cooled down (1 °C/s) to four different deformation temperatures. These four temperatures define the amount of ferrite before the last deformation. To obtain fully austenitic and ferritic microstructures prior to the last pass, deformation temperatures of 800 °C and 650 °C, denominated here as Tdef0 and Tdef100, respectively (0% and 100% of ferrite prior to the last deformation pass), were defined. In the intercritical region, two different deformation temperatures were defined in order to achieve 25 and 75% of ferrite prior to the last deformation (Tdef25 and Tdef75, respectively). For the CMn steel, deformation temperatures of 705 and 685 °C were defined, for Tdef25 and Tdef75, respectively. For the NbV microalloyed steel, higher deformation temperatures of 715 and 700 °C were selected, in order to reach 25 and 75% of ferrite. After reaching the desired ferrite-austenite balance, a deformation of 0.4 was applied in each region: austenitic (Tdef0), intercritical (Tdef25 and Tdef75) or ferritic (Tdef100). Finally, the specimens were cooled down to room temperature at 1 °C/s.

The specimens used for the microstructural and mechanical characterization were obtained from the central part of the plane strain compression samples in order to minimize strain gradients [22]. The characterization of the final microstructures was carried out in samples etched in 2% Nital by optical microscopy using a LEICA DMI5000 M microscope and field-emission gun scanning electron microscopy with a JEOL JSM-7000F. Micrographs in the following pictures are aligned with the compression deformation direction parallel to the vertical axis.

EBSD sample preparation was based on a conventional polishing route, using diamond liquids down to 1 μm, followed by a final polishing with a 50 nm colloidal silica suspension. Orientation imaging microscopy was performed on the Philips XL 30CP SEM with a W-filament, using TSL equipment. A step size of 0.5 μm was defined and an accelerating voltage of 20 kV was used, with a total scanned area of 350 × 350 μm^2. The EBSD scans were analyzed using TSL OIM™ Analysis 5.31 software. Different EBSD discretization parameters were employed to distinguish the constituents formed in the final microstructure (pearlite, non-deformed ferrite and deformed ferrite). To distinguish pearlite from ferrite, an image quality (IQ)-based method was employed [23,24]. The Average IQ threshold values were fixed to each condition based on the pearlite contents measured for each case. The grain orientation spread (GOS) parameter was considered in order to differentiate intercritically deformed ferrite from non-deformed ferrite. In the current study, a GOS tolerance angle of 2° [20] was employed. Ferrite grains with GOS values lower and higher than 2° were considered to be non-deformed and deformed ferrite grains, respectively.

Cylindrical tensile samples (diameter of 4 mm and gauge length of 17 mm) as well as sub-size Charpy specimens (~5.5 × 10 × 55 mm^3 and ~4 × 10 × 55 mm^3, for CMn and NbV respectively) were machined from the central part of the plane compression specimens. Schematics are shown in Fig. 2. The 2% proof stress and the tensile strength were determined by averaging the two tensile tests in each condition. The tensile tests were carried out at room temperature, on an Instron testing machine using a strain rate of 10^{-3} s^{-1}. Charpy tests were carried out in a Tilnius Olsen Model Impact 104 pendulum impact tester for the Tdef0, Tdef25 and Tdef75 conditions. The impact transition curves were defined according to the modified hyperbolic tangent fitting algorithm reported by Wallin [25]. Due to geometrical limitation, sub-size specimens are machined and therefore, the absorbed energy extrapolation to a standard geometry is required. In order to extrapolate the absorbed energy according to the standard, the following equation is used [26]. Specimen thicknesses of 4 and 5.5 mm are within the applicability range of the following proportionality rule:

$$k_{v10} = {}^{10}/_{B} \cdot k_{vB}$$

where k_{v10} and k_{vB} are the absorbed energies for Charpy specimens with a thickness of 10 mm and B (subsize specimen thickness) mm, respectively.

Table 1
Chemical composition of the studied steels (weight percent).

	C	Mn	Si	Cr	V	Ti	Al	Nb	N	S	P	Cu
CMn	0.063	1.53	0.25	0.012	0.005	0.002	0.035	0.002	0.0030	0.003	0.013	0.009
NbV	0.062	1.52	0.25	0.012	0.034	0.002	0.038	0.056	0.0040	0.003	0.013	0.010

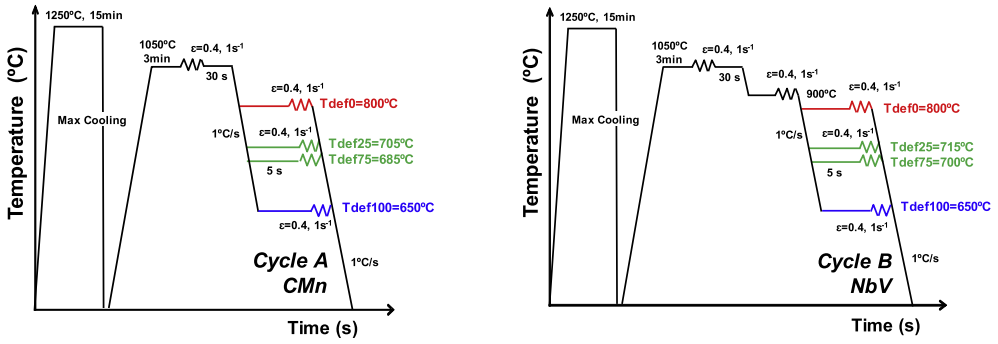

Fig. 1. Thermomechanical cycles applied in plane strain compression tests: (a) Cycle A for CMn and (b) Cycle B for NbV microalloyed steels.

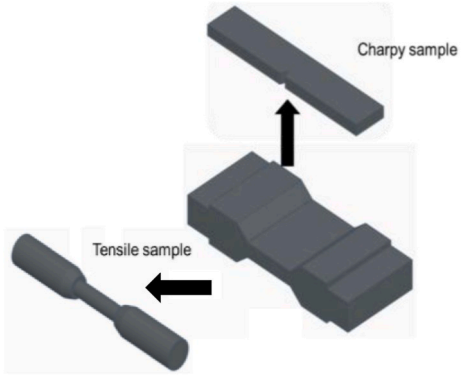

Fig. 2. Schematics of the mechanical property sample extraction from the plane strain compression sample.

3. Results

3.1. Microstructural characterization

Fig. 3 illustrates the differences between the formed microstructures as a function of the deformation temperatures of the last deformation pass for both chemistries (Tdef0, Tdef25, Tdef75 and Tdef100). When the last deformation pass is applied in the austenitic region at 800 °C, as shown in Fig. 3a and e, polygonal ferrite grains in conjunction with pearlite can be distinguished in the resulting microstructure. Within the intercritical region (Tdef25 and Tdef75), combinations of non-deformed and deformed ferrite are clearly noticed in all conditions and the reduction of the deformation temperature leads to the increment of the deformed ferrite content. Furthermore, as the ferrite content prior to intercritical deformation increases, the presence of substructure is more evident, reflecting a higher fraction of deformed ferrite. Conversely, when the last deformation pass is applied at low temperatures in the ferritic region at 650 °C (Tdef100), the microstructure is characterized by the presence of an almost fully deformed ferritic microstructure (see Fig. 3d and h).

The effect of microalloying elements on the microstructural refinement is also evident for all the deformation temperatures studied. Finer ferrite grains can be noticed in the NbV microalloyed grade (see Fig. 3e, f, g and h). In the Nb containing steel, the last deformation applied below T_{nr} promotes the accumulation of deformation on the austenite prior to transformation, significantly increasing the density of ferrite nucleation sites and justifying the refinement of the resulting microstructure [27].

In the FEG-SEM micrographs shown in Fig. 4, the differences between the NDF and DF populations are relevant. For the Tdef25 condition and both steel grades, relatively polygonal microstructures can be distinguished, due to a high fraction of non-deformed ferrite grains. For CMn, a well-defined substructure is noticed inside the DF grains when Tdef75 is applied (see Fig. 4b), which is related to the activation of ferrite restoration mechanisms during deformation in the intercritical region. Slightly different DF morphology can be appreciated when the microstructure corresponding to NbV and Tdef75 is analyzed in Fig. 4d. In this case, the presence of sub-boundaries is less significant and deformation bands can be distinguished in some regions. This could be associated with the delaying of ferrite restoration caused by Nb in solid solution. The solute drag effect that occurs due to the Nb in solution delays the restoration/recrystallization phenomena taking place during intercritical deformation [21].

3.2. Crystallographic characterization by EBSD

Fig. 5 shows several EBSD maps obtained for the CMn steel and different deformed ferrite contents after removing pearlite constituent (Tdef0, Tdef25, Tdef75 and Tdef100, in Fig. 5a, b, c and d, respectively). Black zones in the grain boundary maps correspond to the pearlite areas. In these maps, low angle misorientation boundaries (between 4° and 15°) are represented in red, whereas black lines correspond to high angle boundaries (higher than 15°). As shown in Fig. 5, when the microstructure before deformation is characterized by the lack of ferrite or a low fraction of it, a relatively equiaxed ferritic microstructure is obtained after final air cooling (see Fig. 5a and b), which is associated with a high non-deformed ferrite content. Nevertheless, as the deformation temperature is reduced (Tdef75 and Tdef100), the deformed ferrite content increases (see Fig. 5c and d), leading to the formation of more elongated ferrite grains with a significant substructure (reflected as low angle boundaries drawn in red).

3.3. Tensile and toughness properties

Fig. 6a and b shows tensile curves corresponding to CMn and NbV, respectively, and for the Tdef0, Tdef25, Tdef75 and Tdef100 conditions. Concerning the shape of the curves, most of them show discontinuous yielding behavior although this plateau is less evident in the Tdef100 condition for both steels. In terms of the influence of chemistry, the results plotted in Fig. 6 suggest that the addition of microalloying elements promotes the improvement of tensile properties for all the conditions. For example, for Tdef75, yield strengths (YS) of 337 and 424.4 MPa were measured for the CMn and the NbV steels, respectively. Concerning the effect of final deformation temperature, both yield and tensile strength (TS) increased as this temperature decreases. For both chemistries, the highest YS and TS values were achieved for the lowest deformation temperature of 650 °C. For example, in the microalloyed steel, an improvement of 57 MPa in yield strength was achieved when the deformation temperature was decreased from 800 to 650 °C. Even though tensile property enhancement could be reached by decreasing deformation temperature, the reduction of elongation is significant

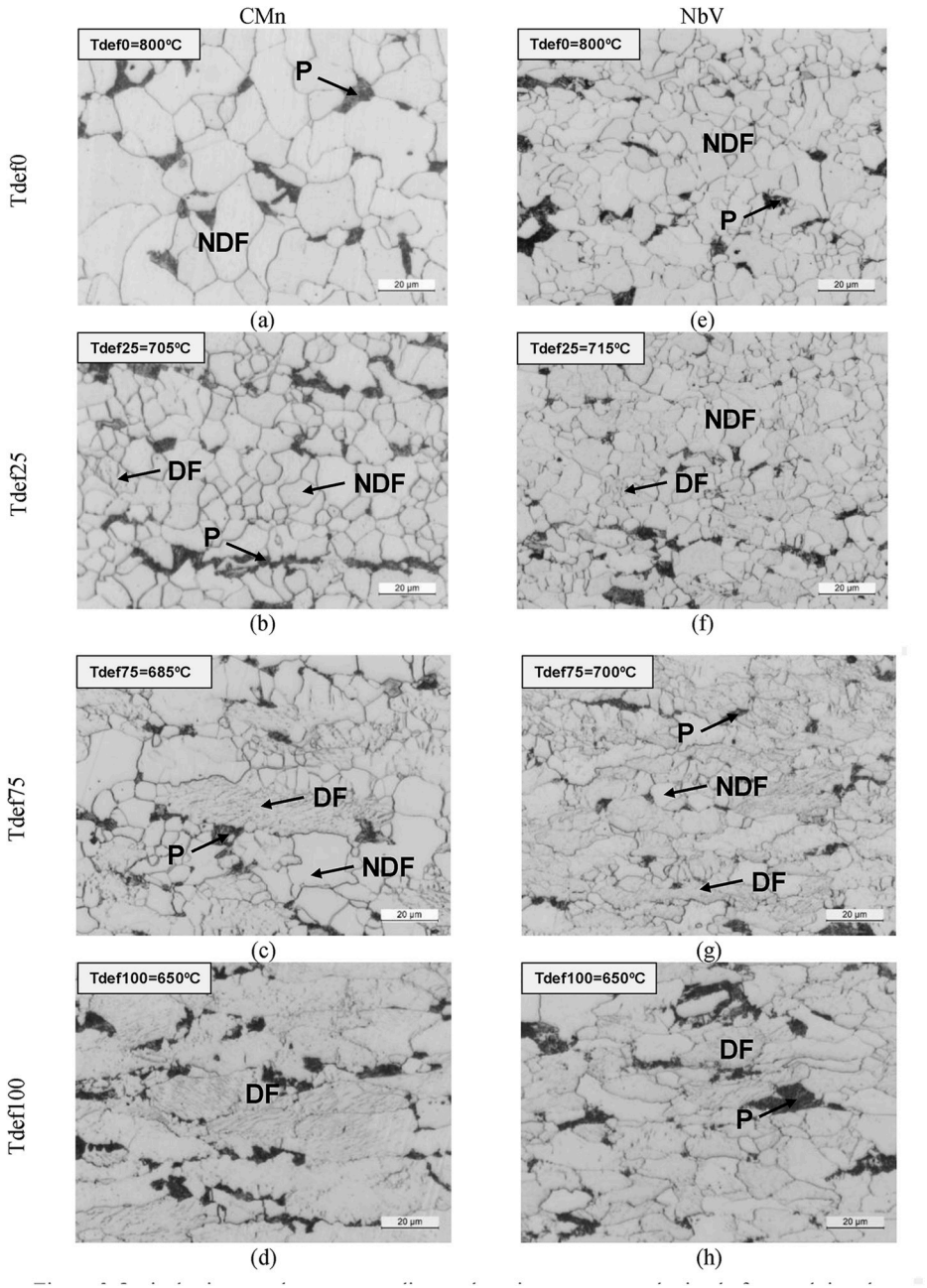

Fig. 3. Optical micrographs corresponding to the microstructures obtained after applying the last deformation pass at different deformation temperatures and both steels: (a,e) Tdef0 (austenitic region), (b,f) Tdef25 (intercritical region, 25% DF), (c,g) Tdef75 (intercritical region, 75% DF) and (d,h) Tdef100 (ferritic region).

when the microstructure contains deformed ferrite fractions higher to 25% (Tdef75 and Tdef100). This trend could be observed in both the CMn and the NbV chemistries. In the CMn steel, the elongation decreases from 47.5 to 26% for Tdef0 and Tdef100, respectively.

Fig. 7 shows the impact transition curves obtained for the CMn (a,b) and the NbV (c,d) steels. In Fig. 7, both the absorbed energy and the ductile fraction are plotted as a function of test temperature. Concerning the effect of the addition of microalloying elements, the addition of Nb and V shifts the impact transition curves to lower temperatures, showing better toughness properties. This could be mainly attributed to the microstructural refinement observed when microalloying elements are added. Regarding the effect of austenite-ferrite balance prior to deformation, for both steels the results suggest that higher transition temperatures are achieved as the last deformation temperature decreases due to the presence of a higher fraction of deformed ferrite. Therefore, as the intercritically deformed ferrite content increases, worse toughness behavior is observed. In the CMn steel, sharp ductile to brittle transitions are observed when the last deformation is applied at 800 °C (Tdef0) and 705 °C (Tdef25), whereas for 685 °C (Tdef75) the transition ranges are wider. These differences could be explained by the presence of a higher content of intercritically deformed ferrite population for the lowest deformation temperature. The influence of deformation temperature is more evident in the CMn steel than in the NbV steel.

4. Discussion

4.1. Differentiation of deformed ferrite from non-deformed ferrite

Fig. 8a and b shows the grain boundary maps corresponding to the non-deformed and deformed ferrite population of the CMn steel,

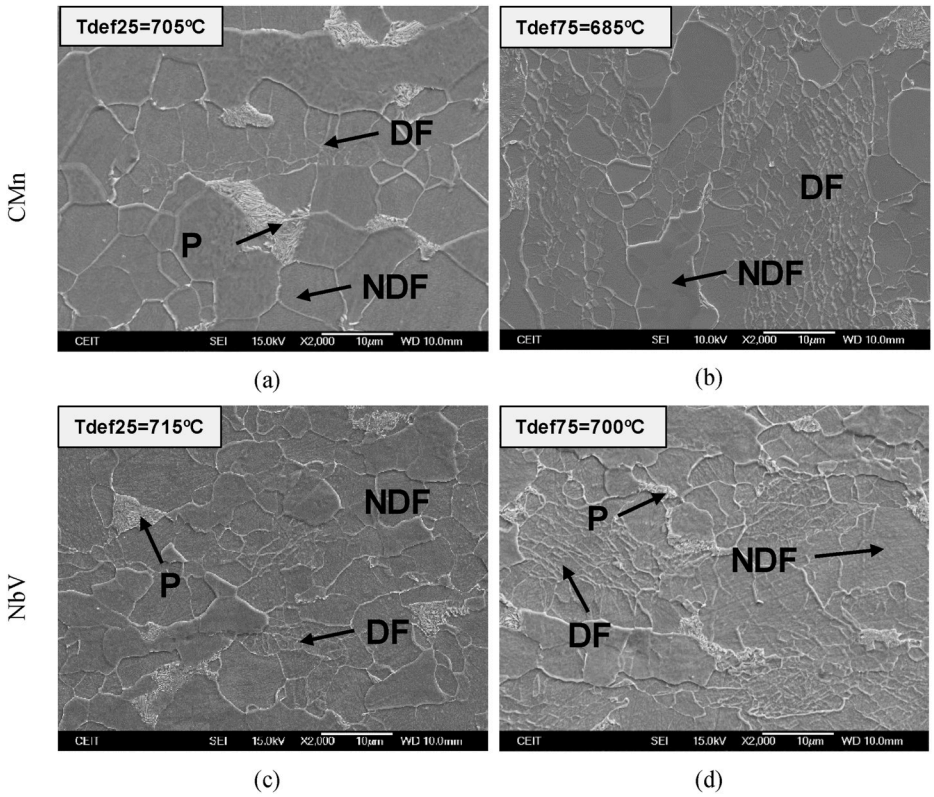

Fig. 4. FEG-SEM images related to the microstructures obtained after applying the last deformation pass in the intercritical region (CMn in a,b and NbV in c,d): (a,c) Tdef25 and (b,d) Tdef75.

discretized by the GOS parameter criterion of 2°. On the other hand, Fig. 8c and d correspond to the Kernel Average Misorientation (KAM) maps of the non-deformed and deformed ferrite family, respectively, obtained in the same conditions. The EBSD map presented in Fig. 8b confirms that intercritically deformed ferrite grains are characterized by the presence of a more evident substructure (see red lines drawn in the grain boundary maps). In addition, in Fig. 8c and d the differences between both ferrite populations become more evident as completely different kernel maps are observed for each ferrite family. Significantly higher KAM values are measured for the population composed of deformed ferrite compared to non-deformed ferrite family. KAM values of 0.9 and 1.3° were quantified, for the non-deformed and deformed ferrite populations, respectively. In the kernel map corresponding to NDF, mainly green-blue colors can be distinguished, while in the deformed ferrite family, the red-colored regions are more noticeable.

In Fig. 9a and b, mean unit size values and KAM values are plotted, respectively. For quantifying the mean grain size, the high angle misorientation criteria was considered, measuring the unit sizes with higher tolerance angle than 15°. Concerning mean unit sizes that was quantified by considering high angle boundaries (see Fig. 9a), the ferrite-austenite balance before deformation affects 15° mean unit size (named as D15), mainly when the non-deformed ferrite population is analyzed. D15 is calculated as the equivalent area diameter. This parameter is usually applied to equiaxed grains but it was proven to be useful for mechanical property quantification for non-polygonal and irregular-shaped crystallographic units [28,29]. The measurements indicate that the reduction of the deformation temperature ensures non-deformed ferrite grain refinement due to a higher ferrite content and therefore a smaller remaining austenite content, promoting the formation of finer microstructures in the final slow cooling. Similarly, the addition of Nb and V promotes the formation of finer NDF and DF grains. For the deformed ferrite family, coarser microstructures are achieved as the deformed ferrite fraction increases. For the NbV steel, D15° of 6.3, 7.9 and 8.3 µm were measured for Tdef25, Tdef75 and Tdef100, respectively.

As plotted in Fig. 9b, the deformed ferrite population presents higher KAM values in the entire range of deformation temperatures. For both non-deformed and deformed ferrite families, the lowest KAM values are achieved in the CMn steel. The increment of kernelvalues caused by addition of microalloying elements could be associated with the formation of quasipolygonal ferritic phases with higher dislocation density. The addition of microalloying elements promotes a delaying of austenite-ferrite transformation, leading to a decrease of the transformation temperatures and the formation of quasipolygonal ferrite instead of polygonal ferrite. Polygonal ferrite (PF) nucleates as grain boundary allotriomorphs, contains by very low dislocation densities and is characterized by the lack of substructure. Growth of polygonal equiaxed ferrite is controlled by rapid substitutional atom transfer across partially coherent boundaries and long-range diffusion of carbon atoms, which are rejected from the growing ferrite. Quasipolygonal ferrite (QF) grains have irregular grain boundaries and a clear substructure [30]. Similar to PF, QF nucleates heterogeneously at the austenite grain boundaries. The transformation can be accomplished by short-range diffusion across transformation interfaces. Interstitial or substitutional atom partitioning may occur at the migrating interfaces, leading to irregular growth and jagged boundaries of massive ferrite crystals. QF is also characterized by higher dislocation densities.

Regarding the effect of deformation temperature, the results plotted in Fig. 9b suggest that the reduction of deformation temperature from Tdef0 to Tdef25 lead to the formation of a NDF family (transformed during final air cooling) with higher KAM values for both chemical compositions. Conversely, for lower deformation temperatures (below Tdef25) for the CMn steel, the kernel parameter remains almost constant. Regarding the DF population, the reduction of deformation temperature promotes a slight increment of the kernel parameter. For example, for the NbV grade, KAM values of 1.3 and 1.5° were quantified

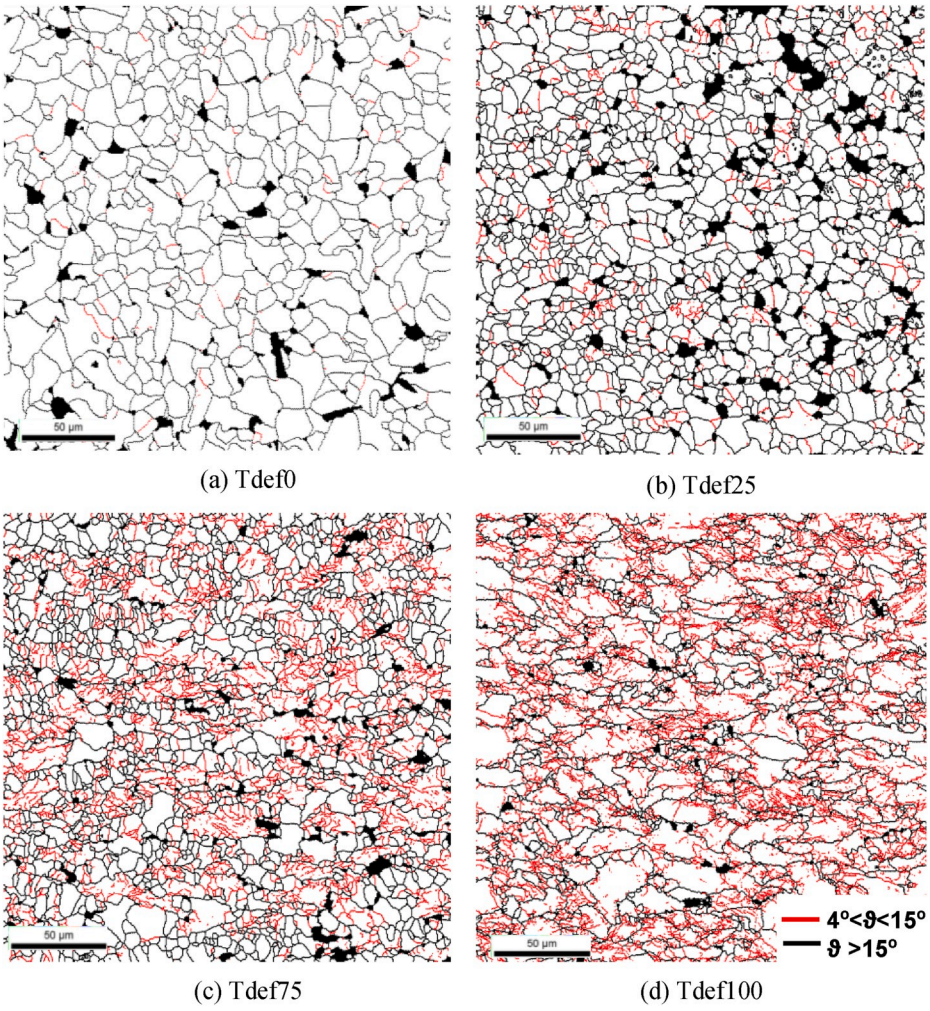

Fig. 5. Grain boundary maps corresponding to CMn and different conditions: (a) Tdef0, (b) Tdef25, (c) Tdef75 and (d) Tdef100.

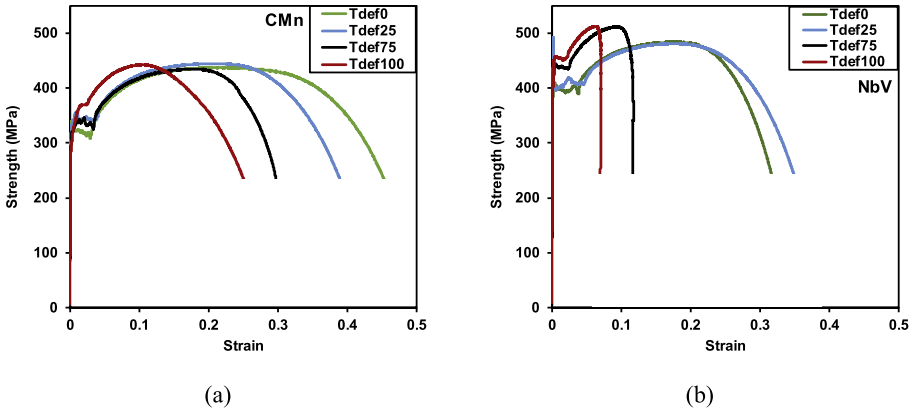

Fig. 6. Comparison between tensile curves obtained after applying the last deformation pass in austenitic region (Tdef0), ferritic region (Tdef100) and intercritical region (Tdef25 and Tdef75) for both chemistries: (a) CMn and (b) NbV microalloyed steel.

for Tdef25 and Tdef75, respectively.

4.2. Estimation of the contribution of strengthening mechanisms to yield strength

Tensile data (yield and tensile strength) corresponding to both steels and the entire range of deformation temperatures are plotted in Fig. 10. Looking at the evolution of yield strength (YS; see Fig. 10a), two strength levels can be clearly distinguished as a function of steel composition. The highest strength levels are reached for the NbV steel, which is attributed to the potential of Nb and V to promote the formation of finer microstructures and quasipolygonal ferritic grains with higher dislocation density. For example, in the CMn steel, YS ranges between 332.5 and 379.4 MPa from Tdef0 to Tdef100, respectively. By contrast, in the

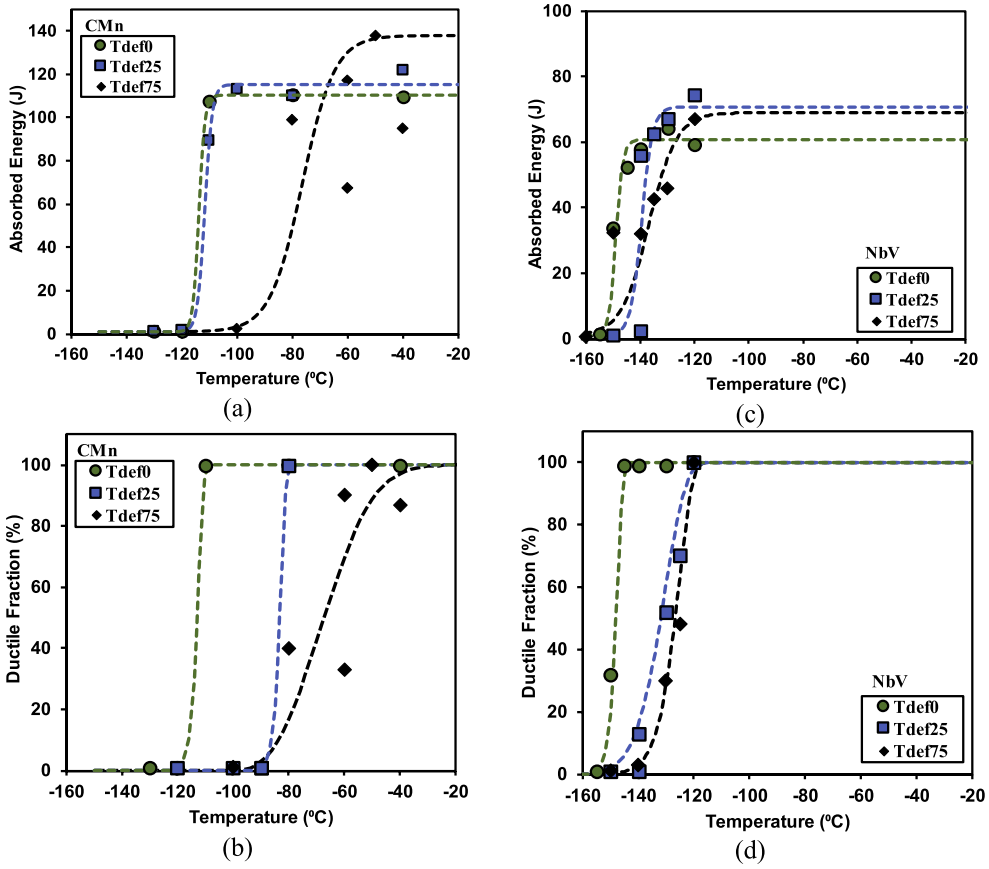

Fig. 7. (a,c) Absorbed energy and (b,d) ductile fraction as a function of test temperature for the entire range of deformation temperatures and chemical compositions: (a,b) CMn and (c,d) NbV.

NbV steel, the yield strength value changes from 403.6 to 460.9 MPa for the same conditions. A similar trend is noticed for the tensile strength (see Fig. 10b). Regarding the effect of deformation temperature, the results plotted in Fig. 10a and b suggest that for NbV, the reduction of deformation temperature leads to the increment of yield and tensile strength values, where the variation of those properties is less relevant for the CMn steel.

In Fig. 10c, the elongation values measured at rupture in each condition are shown. On the one hand, the influence of chemical composition on elongation is clear. Higher elongation values are attained for the CMn steel compared to the NbV steel due to the formation of more polygonal ferritic and softer matrix. On the other hand, as the deformation temperature decreases, elongation reduces significantly, which is associated with the presence of considerably higher deformed ferrite content in the final microstructure. For example, for CMn, the elongation is reduced from 47.5 to 26% for the austenitic 800 °C and the ferritic 650 °C conditions, respectively.

In single phase steels, the yield strength is usually estimated by considering the linear sum of the different strengthening contributions, such as solid solution (σ_{ss}), grain size (σ_{gs}), dislocation density (σ_{ρ}) and fine precipitation (σ_{ppt}). Several works have already considered this linear approach [31–36]. However, for multiphase steels, the hardening of the different constituents has to be considered. Several non-linear approaches have been published in the literature [37–39], in order to take into account the effect of massive aggregate or second-phase hardening. For ferrite-pearlite and ferrite-martensite microstructures, a non-linear law of mixtures is generally employed, as shown in Equation (1) [40]:

$$\sigma_y = f_1^n \sigma_1 + \left(1 - f_1^n\right)\sigma_2 \quad (1)$$

where fi and σi are related to the fraction and the strength of the "i" constituent. For ferrite-pearlite microstructures, the n exponent is considered 1/3.

In the current work, the effect of different strengthening mechanisms on yield strength was evaluated according to Equation (2). f_{NDF} and f_{DF} correspond to non-deformed and deformed ferrite fractions, respectively. To estimate the σ_{ss}, σ_{gs} and σ_{ρ} terms, approaches previously reported in the literature have been used, as shown in Equations (3)–(5) [41,42]. With regard to N_{free}%, for the NbV steel all the nitrogen is considered to be fully precipitated at room temperature. Concerning dislocation density, the contribution of this strengthening mechanism was evaluated through the kernel average misorientation value obtained by EBSD. For NDF, due to the presence of polygonal ferritic grains, the contribution of dislocation density to the strength is considered to be zero. The overestimation in the calculation of dislocation density through kernel average misorientation has already been reported by other authors, mainly for ferritic microstructures [43,44]. Influence of texture in the mechanical properties was neglected in this study. Texture analyses in the current grades based on equivalent deformation sequences revealed that effect of texture formed after intercritical deformation was secondary when compared to grain size refinement, substructure and dislocation density [45,46]. More information regarding the methodology followed can be found in Ref 43:

$$\sigma_y = \sigma_{ss} + \left(\left(f_{NDF}\right)^{1/3} \cdot \left(\sigma_{gs(NDF)} + \sigma_{\rho(NDF)}\right)\right) + \left(\left(1 - \left(f_{NDF}\right)^{1/3}\right) \cdot \left(\sigma_{gs(DF)} + \sigma_{\rho(DF)}\right)\right) \quad (2)$$

$$\text{Solid solution: } \sigma_{ss} = \sigma_0 + 32.3Mn + 83.2Si + 11Mo + 354\left(N_{free}\%\right)^{0.5} \quad (3)$$

$$\text{Grain size: } \sigma_{gs} = 17.4 \cdot d^{-0.5} \quad (4)$$

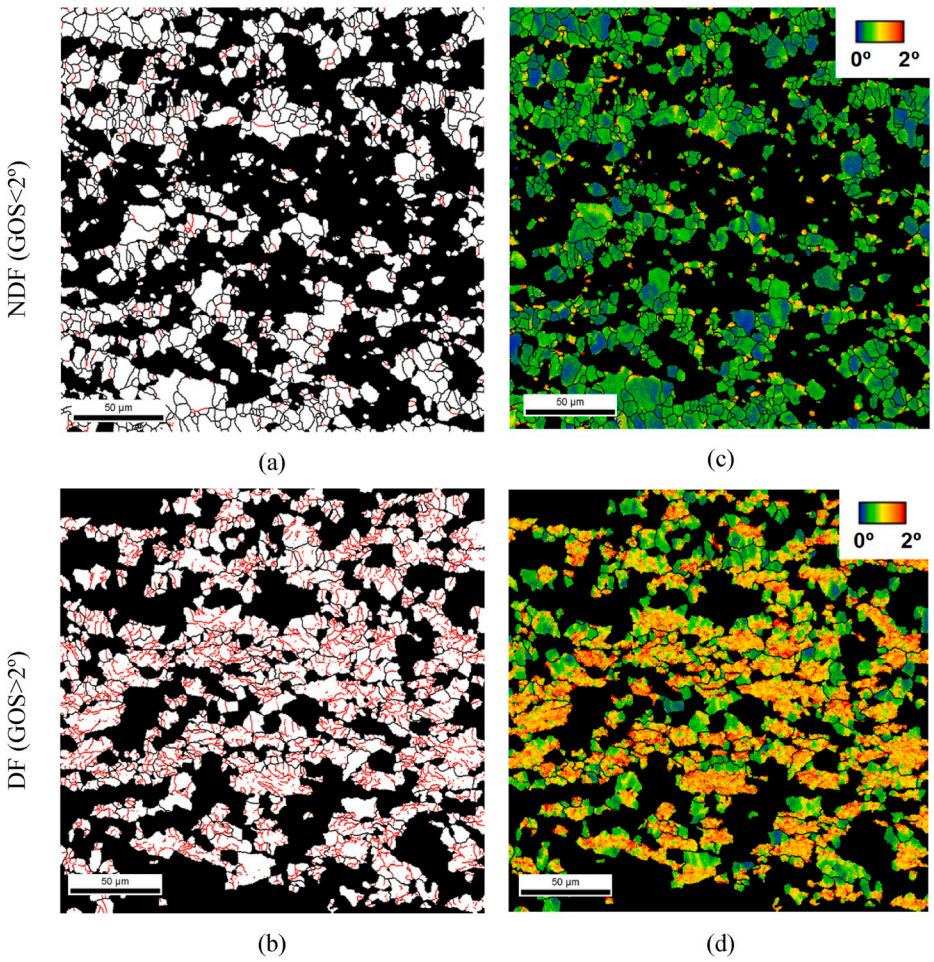

Fig. 8. (a,b) Grain boundary and (c,d) kernel average misorientation maps corresponding to CMn steel for Tdef75 condition and both ferrite families: (a,c) NDF (GOS<2°) and (b,d) DF (GOS>2°).

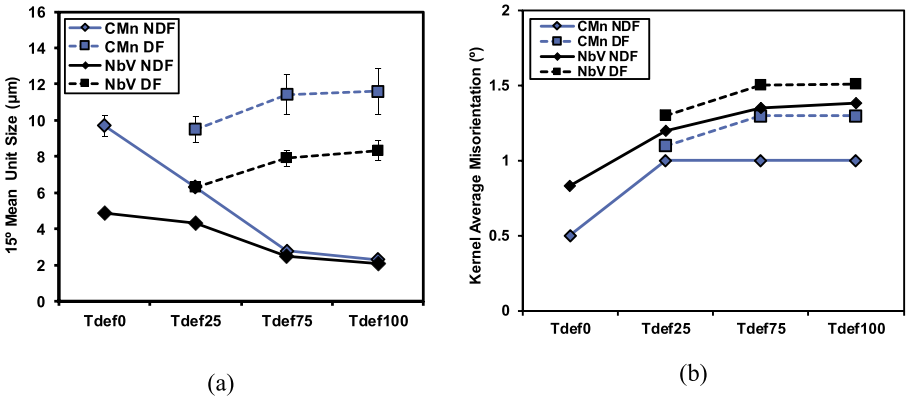

Fig. 9. (a) Mean unit sizes considering high angle boundaries (higher than 15°) and (b) kernel average misorientation values corresponding to NDF and DF populations and different conditions (Tdef0, Tdef25, Tdef75, Tdef100).

Dislocation density: $\sigma_\rho = \alpha M \mu b \sqrt{\rho}$; $\rho = 2\theta/_{ub}$ (5)

The estimated individual strengthening contributions, taking Equation (2) into account, are presented in Fig. 11a, including the experimental yield strength values measured. The results suggest that in all the conditions, the most important strengthening mechanism is related to grain size, followed by solid solution and dislocation density. The hardening due to grain refinement increases as the deformed ferrite fraction increases, mainly in the CMn steel. For example, in the CMn steel, the contribution due to grain size increased from 177 to 233 MPa, for Tdef0 and Tdef100, respectively. Similarly, the reduction of the deformation temperature promotes an increment of the strengthening due to dislocation density. The increment of DF fraction involves an increasing of dislocation density. When the microstructure contains a low deformed ferrite content, the effect of dislocation density is almost negligible.

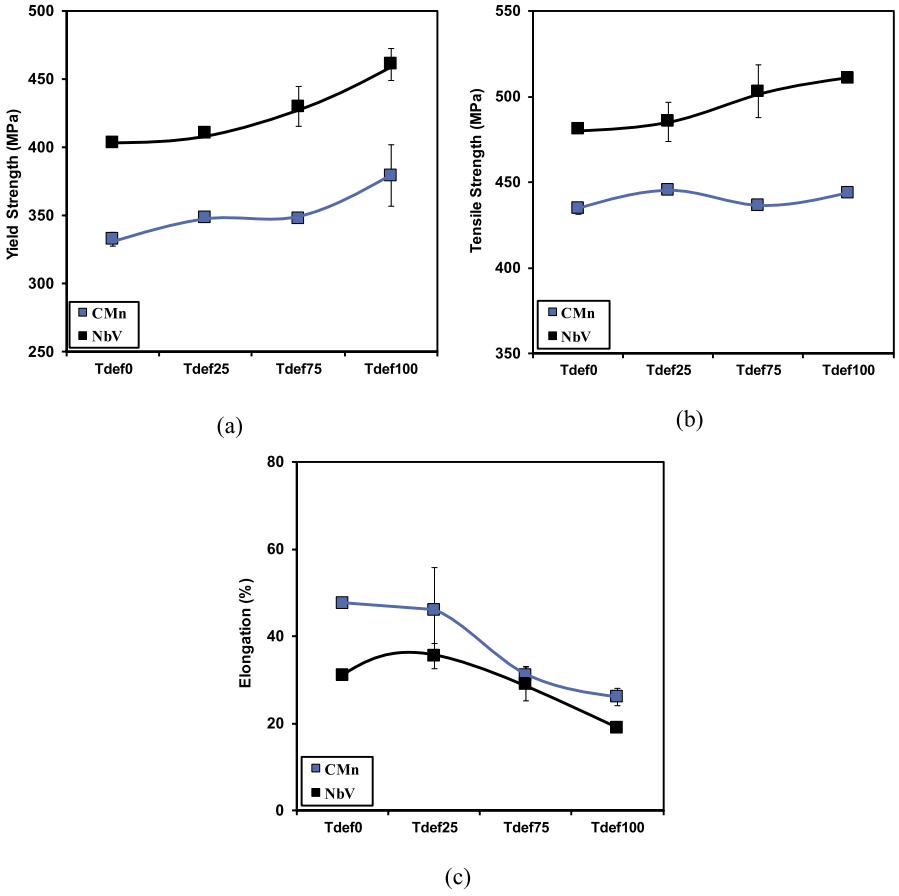

Fig. 10. (a) Yield strength, (b) tensile strength and (c) elongation for all the steels and entire range of deformation temperature.

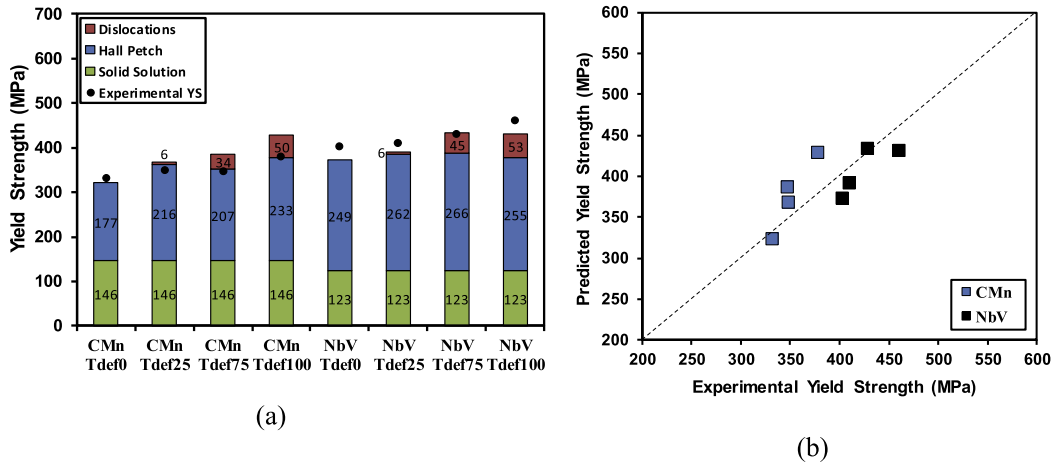

Fig. 11. (a) Contribution of different strengthening mechanism (solid solution, grain size and dislocation density) on the yield strength for both compositions and the full deformation temperature range. (b) Comparison of predicted yield strength considering Equation (2) and experimental yield strength measured by tensile tests for both grades.

For the NbV microalloyed steel, when deformation is applied below the T_{nr}, the formation of strain-induced precipitates is expected, where the typical size is between 10 and 20 nm. Due to the precipitate size, the contribution of strain-induced precipitation to yield strength improvement is considered negligible. Precipitates coarser than 10 nm do not contribute considerably to tensile increase, and therefore the precipitation hardening is limited to particles finer than 10 nm [47]. In a recently published study, a more detailed precipitation analysis was carried out for the same NbV microalloyed steel after a similar thermomechanical cycle [21]. The characterization performed by TEM confirmed that most of the precipitates were formed in the austenitic region. In addition to these strain-induced precipitates, a low density of finer precipitates, which were expected to be formed during or after intercritical deformation, was identified. In this study, a mean

precipitate size of 15.9 nm was measured for Tdef75, and therefore these precipitates can be considered to have a negligible effect on the contribution to yield strength.

In Fig. 11b, the comparison between the experimental and predicted yield strength values obtained from Equation (2) is shown. These results show that a reasonable estimation of yield is achieved for both chemical compositions and the different NDF and DF balances. For the CMn steel and the lower deformation temperatures of Tdef75 and Tdef100, the most significant deviations can be observed comparing experimental and predicted yield strength values. Experimentally lower YS values are measured relative to the ones estimated by Equation (2). In the proposed approach, no effect of restoration of ferrite during intercritical deformation is considered, and therefore the possible softening due to this mechanism is not computed. Thus, the difference between the experimental and calculated YS could be due to the activation of ferrite restoration (observed in the FEG-SEM images shown in Fig. 4a and b).

Regarding the NbV microalloyed steel, for most of the deformation temperatures, slightly higher yield strength values are measured by tensile tests compared to the values estimated by Equation (2). This deviation could be related to the contribution of a low density of fine Nb–V precipitates, which have not been considered and could precipitate in the ferrite during the final air cooling. Anyway, from these results and considering the current cooling rates, the effect of Vanadium strengthening due to fine precipitates is nearly negligible.

4.3. Development of an equation to predict DBTT temperature

Fig. 12a shows 50% ductile to brittle transition temperature (DBTT) values as a function of the last deformation temperature. As mentioned previously, the lowest transition temperatures are measured in the steel containing Nb and V, showing that a microalloying addition ensures improvement in terms of toughness properties. This trend could be attributed to the formation of finer microstructures in the NbV microalloyed steel compared to the CMn steel (see Fig. 9a). Concerning the effect of the last deformation temperature, for both steels higher DBTT values are obtained as deformation temperature decreases, with the worsening of toughness property being more evident for the CMn steel. In this steel, DBTT values of −112, −82 and −66 °C were measured for Tdef0, Tdef25 and Tdef75, respectively.

A new equation for predicting DBTT was proposed recently; it is based on microstructural feature quantification and incorporates the impact of secondary hard phases (such as MA islands) and microstructural heterogeneity on toughness properties [48]:

$$DBTT\,(^{\circ}C) = -11Mn + 42Si + 700\left(N_{free}\%\right)^{0.5} + 15\left(Pearlite\% + MA\%\right)^{1/3} + 0.5\Delta\sigma_y - 14\left(D15^{\circ}\right)^{-0.5} + 39\left(Dc20\%/D15^{\circ}\right)^{0.5} + 23\left(D_{MA}\right)^{0.5} \quad (6)$$

In Equation (6), the first two terms correspond to the solid solution contribution and $N_{free}\%$ is the nitrogen in solid solution. The effect of secondary phases is included through the pearlite and MA (martensite-austenite island) fractions, as well as the MA size (D_{MA}). For heterogeneity evaluation, the ratio between *Dc20%* and *D15°* is included. In a grain size distribution, *Dc20%* is considered as the cutoff grain size at 80% of area fraction [48], i.e. 20% of the grains are bigger than this cutoff grain size. Concerning the contribution of the term associated with fine precipitation and dislocation density, a different impact of $\Delta\sigma y$ as a function of the microstructure morphology was reported. Pickering proposed an effect of 0.45 °C·MPa^{-1} for mainly ferritic microstructures [36], whereas for bainitic phases, in a recently modified DBTT equation the effect decreases to 0.26 °C·MPa^{-1} [29]. In the current study, the effect of $\sigma_\rho + \sigma_{ppt}$ was weighted by a factor of 0.5 °C·MPa^{-1}. The same factor was also previously reported for low carbon microalloyed steels [48,49]. The grain size effect for *D15°* was multiplied by a factor of 14 °C·MPa^{-1}.

To take into account the effective cleavage grain size, D15° is calculated by a mixture law in which the grain sizes corresponding to each ferrite family are considered:

$$D15^{\circ} = D15^{\circ}_{NDF} \cdot f_{NDF} + D15^{\circ}_{DF} \cdot f_{DF} \quad (7)$$

Once the term associated with D15° was extended for intercritically deformed microstructures, a new prefactor for heterogeneity was defined and its detrimental effect on DBTT was reduced. The negative effect of the presence of coarse grain sizes is considered in the modified D15° expression (Eq. (7)), which includes the bimodality of the intercritically deformed microstructures. The modified equation developed for DBTT prediction of intercritically deformed microstructures is shown in Equation (8). In this modified version the effect of MA was not included as MA fraction is negligible in all samples.

$$DBTT\,(^{\circ}C) = -11Mn + 42Si + 700\left(N_{free}\%\right)^{0.5} + 15\left(Pearlite\%\right)^{1/3} + 0.5\Delta\sigma_y - 14\left(D15^{\circ}\right)^{-0.5} + \left(Dc20\%/D15^{\circ}\right)^{0.5} \quad (8)$$

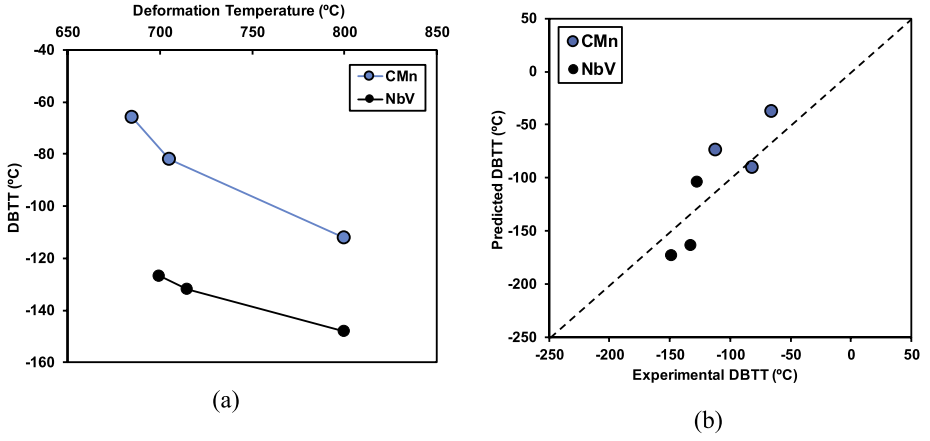

Fig. 12. (a) DBTT as a function of deformation temperature for the CMn and the NbV steels. (b) Comparison between the predicted DBTT through Equation (8) and experimental DBTT obtained by Charpy tests.

Ductile to brittle transition temperatures were estimated according to the proposed Equation (8) and the predicted values have been plotted against the experimental ones in Fig. 12b, yielding reasonable DBTT predictions.

4.4. Relation between tensile and toughness properties

The influence of the different metallurgical parameters on yield strength and DBTT values can be analyzed by vector diagrams equivalent to the ones proposed by Gladman [31]. These diagrams summarize the different strengthening strategies that industry can follow to achieve the required mechanical properties. In Fig. 13a and b, the strengthening/embrittlement terms related to each mechanism and the sum of all the contributions are represented for comparison. The different deformation temperatures (Tdef0, Tdef25 and Tdef75) are represented with different line styles. For both steels, the lowest YS values are predicted for the Tdef0 condition (continuous line), mainly attributed to a coarser grain size. Conversely, the best strength property is estimated for the lowest deformation temperature (Tdef75), principally due to grain size refinement and the increment of the contribution of the dislocation density, which is strictly related to the presence of a high fraction of DF grains in the microstructure. Nb addition plays an important role in the improvement of both the strength and toughness properties, which is mainly related to the grain size refinement. Regarding solid solution, a beneficial effect of this mechanism on yield strength is observed for both steels. Nevertheless, concerning toughness, solid solution affects it differently depending on the chemistry. For the CMn steel, due to free N, the solid solution promotes an improvement in yield strength, while toughness is impaired. By contrast, in the NbV steel, Nb and V are supposed to be combined with N, reducing the free N to zero and avoiding the detrimental effect of this element on toughness. Pearlite content and heterogeneity only affect toughness.

Concerning the effect of deformation temperature and in the case of the NbV steel (see Fig. 13b), yield strength increases as Tdef decreases, whereas the reduction of deformation temperature is harmful in terms of toughness. The differences observed in the DBTT values depending on the deformation temperature are mainly related to slight variations on the grain size refinement and dislocation density. In summary, toughness and strength properties are impaired and the best relation is obtained for the Tdef25 condition in both steels.

5. Conclusions

Reducing deformation temperature enhances the yield and tensile strength in intercritically rolled microstructures, as more DF grains are formed in the final microstructure. This tensile property improvement is mainly related to the presence of a higher low angle grain boundary fraction, as well as a higher dislocation density. The tensile property improvement is more evident in the NbV steel compared to the CMn steel. However, elongation is clearly reduced as deformation temperature decreases because of the formation of a higher DF fraction, this reduction being more relevant at deformation temperatures below Tdef25.

Worse toughness properties are measured as intercritical deformation temperature decreases, related to a higher presence of DF grains. The formation of a higher fraction of DF grains increases the dislocation density and heterogeneity of the microstructure, leading to elevated impact transition temperatures. The worsening in toughness properties is more noticeable in the CMn steel than in the NbV steel. By contrast, the addition of Nb and V shifts the impact transition curves to lower temperatures due to grain size refinement, improving toughness properties.

The Tdef25 condition presents the optimum strength/toughness relation, together with a good ductility due to its homogeneous microstructure.

Data availability statement

The raw/processed data required to reproduce these findings cannot be shared at this time as the data also forms part of an ongoing study.

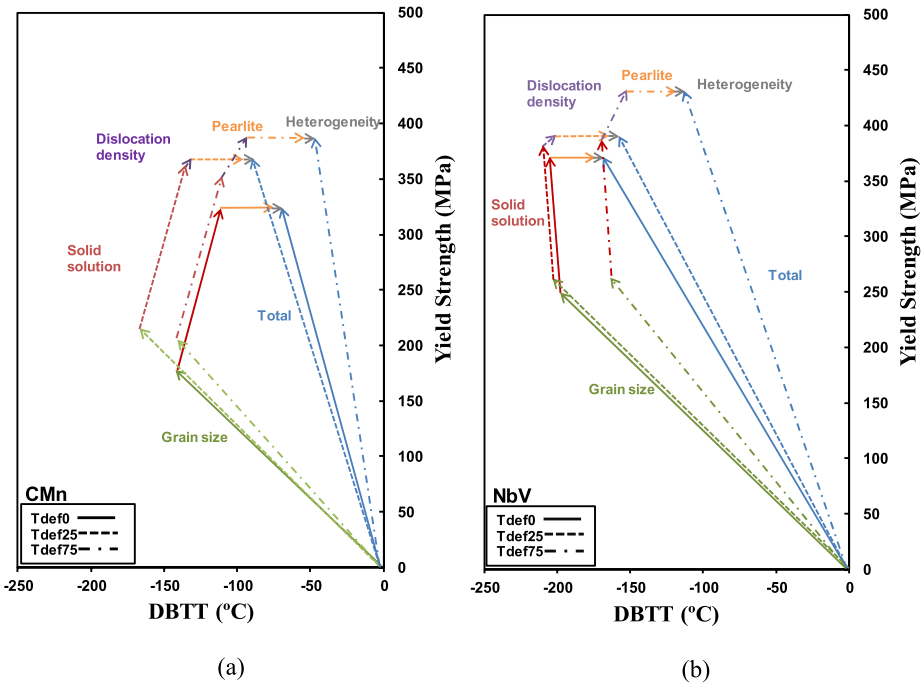

Fig. 13. Representation of the relative contribution of different strengthening mechanisms (grain size, solid solution, dislocation density, pearlite and heterogeneity) on both strength and toughness properties corresponding to (a) CMn and (b) NbV steel for Tdef0, Tdef25 and Tdef75 conditions.

Declaration of competing interest

The authors declare that they have no known competing financial interests or personal relationships that could have appeared to influence the work reported in this paper.

CRediT authorship contribution statement

U. Mayo: Investigation, Writing - original draft, Visualization. **N. Isasti:** Methodology, Validation, Formal analysis, Writing - review & editing. **J.M. Rodriguez-Ibabe:** Conceptualization, Writing - review & editing. **P. Uranga:** Conceptualization, Writing - review & editing, Supervision, Project administration, Funding acquisition.

Acknowledgements

The financial support of the Spanish Ministry of Economy and Competitiveness (MAT2015-69752) is gratefully acknowledged. The authors also acknowledge a research grant from the European Commission Research Fund for Coal and Steel (RFSR-CT-2015-00014).

Appendix A. Supplementary data

Supplementary data to this article can be found online at https://doi.org/10.1016/j.msea.2020.139800.

References

[1] S. Gohda, K. Watanabe, Y. Hashimoto, Effects of the intercritical rolling on structure and properties of low carbon steel, Trans. ISIJ 21 (1981) 6–15, https://doi.org/10.2355/isijinternational1966.21.6.
[2] G.R. Speich, D.S. Dabkowski, Effect of deformation in the austenite and austenite-ferrite regions on the strength and fracture behaviour of C, C-Mn-Cb and C-Mn-Mo-Cb steels, in: J.B. Ballance, AIME (Eds.), Proceedings of the the Hot Deformation of Austenite Conference, 1979, pp. 557–597.
[3] G. Li, T.M. Maccagno, D.Q. Bai, J.J. Jonas, Effect of initial grain size on the static recrystallization kinetics of Nb microalloyed steels, ISIJ Int. 36 (1996) 1479–1485, https://doi.org/10.2355/isijinternational.36.1479.
[4] J.P. Sah, G.J. Richardson, C.M. Sellars, Grain size effects during dynamic recrystallization of nickel, Met. Sci. J. 8 (1974) 325–331, https://doi.org/10.1179/msc.1974.8.1.325.
[5] A. I. Fernandez, PhD Thesis, Universidad de Navarra, 2001.
[6] J.W. Bowden, F.H. Samuel, J.J. Jonas, Effect of interpass time on austenite grain refinement by means of dynamic recrystallization of austenite, Metall. Trans. A 22 (1991) 2947–2957, https://doi.org/10.1007/BF02650254.
[7] A.I. Fernández, P. Uranga, B. López, J.M. Rodriguez-Ibabe, Dynamic recrystallization behavior covering a wide austenite grain size range in Nb and Nb-Ti microalloyed steels, Mater. Sci. Eng. 361 (2003) 367–376, https://doi.org/10.1016/S0921-5093(03)00562-8.
[8] C.M. Sellars, Hot Working and Forming Processes, 1980, p. 3.
[9] O. Kwon, A.J. DeArdo, Interactions between recrystallization and precipitation in hot-deformed microalloyed steels, Acta Metall. Mater. 39 (1991) 529–538, https://doi.org/10.1016/0956-7151(91)90121-G.
[10] B. Eghbali, Microstructural development in a low carbon Ti-microalloyed steel during deformation within the ferrite region, Mater. Sci. Eng. 480 (2008) 84–88, https://doi.org/10.1016/j.msea.2007.06.084.
[11] E.A. Simielli, S. Yue, J.J. Jonas, Recrystallization kinetics of microalloyed steels deformed in the intercritical region, Metall. Trans. A 23 (1992) 597–608, https://doi.org/10.1007/BF02801177.
[12] Y. Saito, Mathematical model of hot deformation resistance in austenite-ferrite two phase region, Trans. ISIJ 27 (1987) 419–424, https://doi.org/10.2355/isijinternational1966.27.419.
[13] H. Luo, J. Sietsma, S. van der Zwaag, A novel observation of strain-induced ferrite to austenite retransformation after intercritical deformation of C-Mn steel, Metall. Mater. Trans. 35 A (2004) 2789–2797, https://doi.org/10.1007/s11661-004-0225-2.
[14] A. Mohamadizadeh, A. Zarei-Hanzaki, S. Mehtonen, Correlation of strain accommodation factor with the state of microstructural components in a multiphase steel, ISIJ Int. 55 (2015) 2406–2415, https://doi.org/10.2355/isijinternational.ISIJINT-2015-213.
[15] L. Hao, M. Sun, N. Xiao, D. Li, Characterizations of dynamic strain-induced transformation in low carbon steel, J. Mater. Sci. Technol. 28 (2012) 1095–1101, https://doi.org/10.1016/S1005-0302(12)60178-9.
[16] Y. Tian, L. Zhao, N. Park, N. Tsuji, A. Shibata, Dynamic Transformation mechanism for producing ultrafine grained steels, Adv. Eng. Mater. 20 (2018) 1701016, https://doi.org/10.1002/adem.201701016.
[17] A. Bodin, J. Sietsma, S. van der Zwaag, On the nature of the bimodal grain size distribution after intercritical deformation of a carbon–manganese steel, Mater. Char. 47 (2001) 187–193.
[18] T. Nguyen-Minh, M. Caruso, I. Tolleneer, U. Mayo, N. Isasti, P. Uranga, U. Lorenz, L. Duprez, F.H. Akbary, R. Petrov, J. Sietsma, Impact of Two-Phase Region Rolling on the Microstructure and Properties Distribution in Heavy Gauge Structural Steel Plate (INCROHSS), Directorate-General for Research and Innovation (European Commission), Publications Office of the European Union, Luxembourg, 2020. In press.
[19] M. Caruso, U. Lorenz, T. Nguyen Minh, P. Uranga, U. Mayo, N. Isasti, R. Petrov, Intercritical rolling of heavy-gauge structural plates: which compromise between strength and toughness?, in: MSE Congress, 26-28 September, 2018 (Darmstadt, Germany).
[20] U. Mayo, N. Isasti, D. Jorge-Badiola, J.M. Rodriguez-Ibabe, P. Uranga, An EBSD-based methodology for the characterization of intercritically deformed low carbon steel, Mater. Char. 147 (2019) 31–42, https://doi.org/10.1016/j.matchar.2018.10.014.
[21] U. Mayo, N. Isasti, J.M. Rodriguez-Ibabe, P. Uranga, Interaction between microalloying additions and phase transformation during intercritical deformation in low carbon steels, Metals 9 (2019) 1049, https://doi.org/10.3390/met9101049.
[22] P. Uranga, I. Gutiérrez, B. López, Determination of recrystallization kinetics from plane strain compression tests, Mater. Sci. Eng. 578 (2013) 174–180, https://doi.org/10.1016/j.msea.2013.04.077.
[23] R. Petrov, L. Kestens, Y. Houbaert, Characterization of the microstructure and transformation behaviour of strained and nonstrained austenite in Nb-V-alloyed C-Mn steel, Mater. Char. 53 (2004) 51–61, https://doi.org/10.1016/j.matchar.2004.07.005.
[24] S.I. Wright, M.M. Nowell, EBSD Image quality mapping, Microsc. Microanal. 12 (2006) 72–84, https://doi.org/10.1017/S1431927606060090.
[25] K. Wallin, Modified Tank Fitting Algorithm for Charpy Impact Data; Research Seminar on Economical and Safe Application of Modern Steels for Pressure Vessels, Aachen, Germany, 2003.
[26] K. Wallin, Upper shelf energy normalisation for sub-sized charpy V specimens, Int. J. Pres. Ves. Pip. 78 (2001) 463–470.
[27] R. Bengochea, B. Lopez, I. Gutierrez, Microstructural evolution during the austenite to ferrite transformation from deformed austenite, Metall. Mater. Trans. 29 (1998) 417–426, https://doi.org/10.1007/s11661-998-0122-1.
[28] N. Isasti, D. Jorge-Badiola, M.L. Taheri, P. Uranga, Microstructural features controlling mechanical properties in Nb-Mo microalloyed steels. Part I: yield strength, Metall. Mater. Trans. 45 (11) (2014) 4960–4971, https://doi.org/10.1007/s11661-014-2450-7.
[29] G. Larzabal, N. Isasti, J. Rodriguez-Ibabe, P. Uranga, Evaluating strengthening and impact toughness mechanisms for ferritic and bainitic microstructures in Nb, Nb-Mo and Ti-Mo microalloyed steels, Metals 7 (2017) 65, https://doi.org/10.3390/met7020065.
[30] G. Krauss, S.W. Thompson, Ferritic microstructures in continuously cooled low- and ultralow-carbon steels, ISIJ Int. 35 (1995) 937–945.
[31] T. Gladman, D. Dulieu, I.D. McIvor, Structure-property relationships in high strength microalloyed steels, Microalloying 75 (1975) 32–55.
[32] B. Mintz, W.B. Morrison, A. Jones, Influence of carbide thickness on impact transition temperature of ferritic steels, Met. Technol. 6 (1979) 252–260, https://doi.org/10.1179/030716979803276246.
[33] P. Choquet, P. Fabregue, J. Giusti, B. Chamont, J.N. Pezant, F. Blanchet, Modelling forces, structure and final properties during the hot rolling process on the hot strip mill, in: International Symposium Mathematical Modelling of Hot Rolling of Steels, 1990, pp. 34–43.
[34] B. Mintz, G. Peterson, A. Nassar, Structure-property relationships in ferrite-pearlite steels, Ironmak. Steelmak. 21 (1994) 215–222.
[35] P.D. Hodgson, R.K. Gibbs, A mathematical model to predict the mechanical properties of hot rolled C-Mn and microalloyed steels, ISIJ Int. 32 (1992) 329–338, https://doi.org/10.2355/isijinternational.32.1329.
[36] F.B. Pickering, Physical Metallurgy and Design of Steels. Barking, Applied Science Publishers, Essex, United Kingdom, 1978.
[37] T. Gladman, I.D. McIvor, F.B. Pickering, Some aspects of the structure-property relationships in high-carbon ferrite-pearlite steels, J. Iron Steel Inst. 10 (1972) 916–930.
[38] J. Majta, R. Kuziak, M. Pietrzyk, H. Krzton, Use of the computer simulation to predict mechanical properties of C-Mn steel after thermomechanical process, J. Mater. Process. Technol. 66 (1996) 581–588, https://doi.org/10.1016/0924-0136(96)02390-4.
[39] J. Kusiak, R. Kuziak, Modelling of microstructure and mechanical properties of steel using the artificial neural network, J. Mater. Process. Technol. 127 (2002) 115–121, https://doi.org/10.1016/S0924-0136(02)00278-9.
[40] J.M. Rodriguez-Ibabe, Metallurgical aspects of rolling process, in: The Making, Shaping and Treating of Steels, Flat Product, AIST, 2014, pp. 113–170.
[41] F.B. Pickering, T. Gladman, Metallurgical Developments in Carbon Steels, Special Report No. 81, Iron and Steel Institute, London, UK, 1963.
[42] L.P. Kubin, A. Mortensen, Geometrically necessary dislocations and strain-gradient plasticity: a few critical issues, Scripta Mater. 48 (2003) 119–125, https://doi.org/10.1016/S1359-6462(02)00335-4.
[43] L. García-Sesma, B. López, B. Pereda, Effect of coiling conditions on the strengthening mechanisms of Nb microalloyed steels with high Ti addition levels, Mater. Sci. Eng. 748 (2019) 386–395, https://doi.org/10.1016/j.msea.2019.01.105.
[44] L. Sanz, B. Pereda, B. López, Effect of thermomechanical treatment and coiling temperature on the strengthening mechanisms of low carbon steels microalloyed

with Nb, Mater. Sci. Eng. 685 (2017) 377–390, https://doi.org/10.1016/j.msea.2017.01.014.
[45] T. Nguyen-Minh, M. Caruso, U. Lorenz, J. Sietsma, R. Petrov, Texture evolutions in heavy gauge steel plates after intercritical rolling at high temperatures, in: MSE Congress 2018, September 26-28, 2018 (Darmstadt, Germany).
[46] M. Caruso, U. Lorenz, T. Nguyen-Minh, P. Uranga, R. Petrov, Impact of intercritical rolling on the strength/toughness balance in heavy gauge structural steel plates, in: THERMEC 2018, July 9-13, 2018 (Paris, France).
[47] W.B. Lee, S.G. Hong, C.G. Park, S.H. Park, Carbide precipitation and high-temperature strength of hot-rolled high-strength, low-alloy steels containing Nb and Mo, Metall. Mater. Trans. 33 (2002) 1689–1698, https://doi.org/10.1007/s11661-002-0178-2.
[48] N. Isasti, D. Jorge-Badiola, M.L. Taheri, P. Uranga, Microstructural features controlling mechanical properties in Nb-Mo microalloyed steels. Part II: impact toughness, Metall. Mater. Trans. 45 (11) (2014) 4972–4982, https://doi.org/10.1007/s11661-014-2451-6.
[49] I. Gutiérrez, Effect of microstructure on the impact toughness of Nb-microalloyed steel: generalisation of existing relations from ferrite-pearlite to high strength microstructures, Mater. Sci. Eng. 571 (2013) 57–67, https://doi.org/10.1016/j.msea.2013.02.006.